ACS OMEGA

Open Access

http://pubs.acs.org/journal/acsodf

Article

Accurate *Ab Initio* Investigation of Electronic and Radiative Properties, and Cross Sections for Charged Diatomic Systems $FrLi^+$ and $FrNa^+$

Chedli Ghanmi* and Hamid Berriche*

Cite This: *ACS Omega* 2023, 8, 44977−44987

Read Online

ACCESS | Metrics & More | Article Recommendations

ABSTRACT: This paper presents an extensive *ab initio* investigation of the electronic properties and elastic collisions of charged diatomic systems $FrLi^+$ and $FrNa^+$. We employ an accurate *ab initio* approach using nonempirical pseudopotentials for Li^+, Na^+, and Fr^+ cores. We calculate the potential energy curves of the ground state and low-lying excited states of $^2\Sigma^+$, $^2\Pi$, and $^2\Delta$ symmetries, identifying and interpreting avoided crossings between higher $^2\Sigma^+$ and $^2\Pi$ states. The spectroscopic parameters, transition dipole moments, and vibrational energies associated with $1-3^2\Sigma^+$ states are calculated, along with the radiative lifetimes of the vibrational states trapped in the $2^2\Sigma^+$ state. Using accurate potential energy data, we evaluate partial and total cross sections across a wide range of energies. At low energies (<1 mK), the elastic cross section follows the Wigner law threshold comportment, while at high energies, it scales as $E^{-1/3}$. To the best of our knowledge, no theoretical or experimental data have been collected on these charged diatomic systems until now. Hence, we proceeded to analyze our findings by comparing them with data acquired from comparable systems. The information pertaining to electronic structures, spectroscopic parameters, transition properties, and collision data provided in this work is expected to serve as a valuable guideline for future theoretical and experimental research on each considered system.

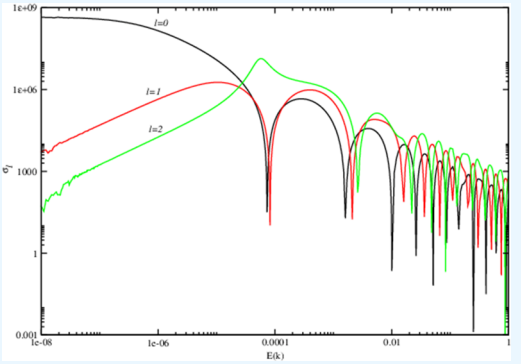

1. INTRODUCTION

Charged diatomic systems composed of alkali metals have been extensively investigated in numerous theoretical works.[1−16] The advancements in experimental techniques for producing cold and ultracold diatomic molecules have opened up new ways for manipulating and controlling their dynamics. Consequently, accurate and detailed spectroscopic information, including dissociation energies, potential energy surfaces, dipole functions, radiative properties, and long-range interaction forces, has become essential. However, the structural and spectroscopic properties of the neutral and ionic alkali diatomic systems containing a francium atom have not been thoroughly examined. Lim et al.[17] carried out the first theoretical investigation of these systems, where they employed coupled cluster and density functional theory to examine the spectroscopic characteristics of neutral alkali dimers ranging from K_2 to Fr_2, along with their corresponding positively charged counterparts. Deiglmayr et al.[18] used the finite-field method to extract the static dipole polarizabilities of homonuclear alkali dimers from Li_2 to Fr_2 from the electronic energies. Aymar et al.[19] employed the pseudopotential method to study the electronic characteristics of alkali molecules, including Fr_2, RbFr, and CsFr, alongside their corresponding cations, for the first time. They successfully obtained potential energy surfaces and spectroscopic constants as well as dipole moments. In a separate investigation, Jendoubi et al.[20] examined the structure and spectroscopic properties of the FrRb system, employing both adiabatic and quasi-diabatic representations. Their investigation employed a standard quantum chemistry approach that relied on the pseudopotential method, Gaussian basis sets, and full configuration interaction calculations. Within the same context, the adiabatic and diabatic electronic properties of the alkali dimers FrLi,[21] FrNa,[22] FrCs,[23] and the francium hydride FrH[24] have also been investigated. In a recent study, Shandalau et al.[25] conducted a theoretical investigation focusing on the radiative and spectroscopic properties of various electronic states of the FrLi molecule. Additionally, they developed models to analyze the optical cycles of the FrLi heteronuclear system.

The current work builds upon our previous theoretical investigations[7−16,20,26−34] concerning the structural and

Received: August 29, 2023
Revised: October 12, 2023
Accepted: October 13, 2023
Published: November 15, 2023

spectroscopic properties of neutral and charged diatomic molecules composed of alkali and alkaline earth atoms. In this article, we extend our calculations to study the electronic properties and elastic collisions of the charged diatomic systems $FrLi^+$ and $FrNa^+$ using the same method. So, previously, the electronic properties of the lowest states of $Fr2^{+19}$, $FrRb^{+19}$, and $FrCs^{+19,23}$ were determined. As far as we are aware, no theoretical or experimental data have been published yet on the $FrLi^+$ and $FrNa^+$ systems. Hence, our work can be regarded as the first study of these charged diatomic systems. This paper is organized as follows: Section 2 offers a brief overview of the computational method used. Section 3 reports the potential energy curves of select electronic states, spectroscopic parameters, vibrational energy, transition dipole moments, and elastic scattering properties. The final section summarizes the key conclusions.

2. CALCULATION METHODOLOGY

The electronic calculations were determined by employing the nonempirical pseudopotential, as suggested by Barthelat et al.,[35] in its semilocal form to simulate the charged diatomic systems FrX^+ (X = Li and Na). These systems are treated as having a single valence electron. Additionally, in accordance with the approach proposed by Müller et al.,[36] the polarizable cores Li^+, Na^+, and Fr^+ are considered to interact with the valence electron through the nucleus polarization potential V_{CPP}

$$V_{CPP} = -\frac{1}{2}\sum_{\lambda} \alpha_\lambda \vec{f}_\lambda \vec{f}_\lambda \tag{1}$$

Here, $\vec{f}_\lambda$ represents the electric field generated by the valence electron and all other cores on the core λ, while α_λ symbolizes the dipole polarizability of the core λ. The electric field $\vec{f}_\lambda$ is given by the following relationship

$$\vec{f}_\lambda = \sum_i \frac{\vec{r}_{i\lambda}}{r_{i\lambda}^3} F(\vec{r}_{i\lambda}, \rho_\lambda) - \sum_{\lambda' \neq \lambda} \frac{\vec{R}_{\lambda'\lambda}}{r_{\lambda'\lambda}^3} Z_\lambda \tag{2}$$

where $\vec{R}_{\lambda'\lambda}$ represents the core−core vector and $\vec{r}_{i\lambda}$ is the core−electron vector.

Based on the formalism introduced by Foucrault et al.,[37] the selection of the cutoff function depends on the value of l, allowing for differentiation in the interaction between valence electrons with different spatial symmetries and core electrons.

$$F(\vec{r}_{i\lambda}, \rho_\lambda) = \sum_{l=0}^{\infty} \sum_{m=-l}^{+l} F_l(r_{i\lambda}, \rho_\lambda^l) |lm\lambda\rangle\langle lm\lambda| \tag{3}$$

where $|lm\lambda\rangle$ represents the spherical harmonic centered on λ, while $F_l(r_{i\lambda},\rho_\lambda^l)$ denotes the cutoff operator, defined as a step function following the formalism of Foucrault et al.[37]

$$F_l(r_{i\lambda}, \rho_\lambda^l) = \begin{cases} 0, & r_{i\lambda} < \rho_\lambda \\ 1, & r_{i\lambda} > \rho_\lambda \end{cases} \tag{4}$$

In the formalism introduced by Müller et al.,[36] the cutoff function excludes the valence electrons from the core region when computation of the electric field. This cutoff function is specific to each atom, and its adjustments are commonly made to accurately replicate the atomic energy levels corresponding to the lowest states of the lowest states within each symmetry. Table 1, presents the polarizabilities of Li^+, Na^+, and Fr^+, along with the respective cutoff values of the lowest one-electron states s, p, and d orbitals in Li, Na, and Fr atoms. The extended basis sets used for the lithium, sodium, and francium are (9s8p5d1f/8s6p3d1f),[8] (7s6p5d3f/6s5p4d2f),[8] and (9s9p9d),[19] respectively. The calculated energies (in cm^{-1}) for Li(2s, 2p, 3s, 3p, and 3d), Na(3s, 3p, 4s, 3d, and 4p) and Fr (7s, 7p, 6d, 8s, and 8p) atomic levels show excellent agreement with experimental[38] values. The results, including the difference (ΔE) between our energy values and the experimental energies, are presented in Table 2.

Table 1. Polarizabilities and Cutoff Parameters for Lithium, Sodium, and Francium Atoms (in a. u.)

atom	α	ρ_s	ρ_p	ρ_d
Li(Z = 3)	0.1915	1.434	0.982	0.600
Na(Z = 11)	0.993	1.4423	1.625	1.500
Fr(Z = 87)	20.38	3.16372	3.045	3.1343

Table 2. Theoretical Atomic Energies of Lithium, Sodium, and Francium Atoms (in cm^{-1}) Compared with Experimental Values[a]

atom	level	this work	experimental (38)	ΔE
Li	2s	−43487.00	−43487.00	0.00
	2p	−28581.79	−28583.32	−1.53
	3s	−16275.16	−16281.09	−5.93
	3p	−12560.99	−12561.87	−0.88
	3d	−12200.83	−12204.12	−4.25
Na	3s	−41449.82	−41449.65	0.17
	3p	−24482.21	−24482.00	0.21
	4s	−15710.67	−15709.79	0.88
	3d	−12276.11	−12276.78	−0.67
	4p	−11177.64	−11179.02	−1.38
Fr	7s	−32848.82	−32848.87	0.05
	7p	−19487.18	−19487.07	0.11
	6d	−16470.94	−16471.25	0.31
	8s	−13136.89	−13116.39	−20.50
	8p	−9424.91	−9372.35	−52.56

[a] ΔE represents the differences between our *ab initio* data and the experimental energies.

3. RESULTS AND DISCUSSION

3.1. Potential Energy Curves and Spectroscopic Parameters. Applying the Born−Oppenheimer approximation, we calculated the adiabatic potential energy curves of charged diatomic systems, specifically $FrLi^+$ and $FrNa^+$, for various electronic states with symmetries including $^2\Sigma^+$, $^2\Pi$, and $^2\Delta$. These curves were obtained over a dense grid of interatomic distances spanning from 4.00 to 150.00 au. Figure 1 displays the adiabatic potential energy curves for 18 states of the charged systems $FrLi^+$ dissociating up to Fr (8p) + Li^+ and Fr^+ + Li(3d). Figure 2 shows the results for $FrNa^+$ dissociating up to Fr (8p) + Na^+ and Fr^+ + Na(4p). For both systems, the adiabatic potential energy curves exhibit similar characteristics, wherein the ground state manifests the most profound potential well depth in contrast to that of the other states. Moreover, we observed that the excited states $9^2\Sigma^+$, $3^2\Pi$, $5^2\Pi$, and $1-2^2\Delta$ of $FrLi^+$, and $3^2\Pi$, $5^2\Pi$, and $1-2^2\Delta$ of $FrNa^+$ are found repulsive. Additionally, for higher electronic states, we observed avoided crossings between the adiabatic potential energy curves of $^2\Sigma^+$ symmetry at large distances. Similar behavior has been documented in previous investigations

https://doi.org/10.1021/acsomega.3c06338
ACS Omega 2023, 8, 44977−44987

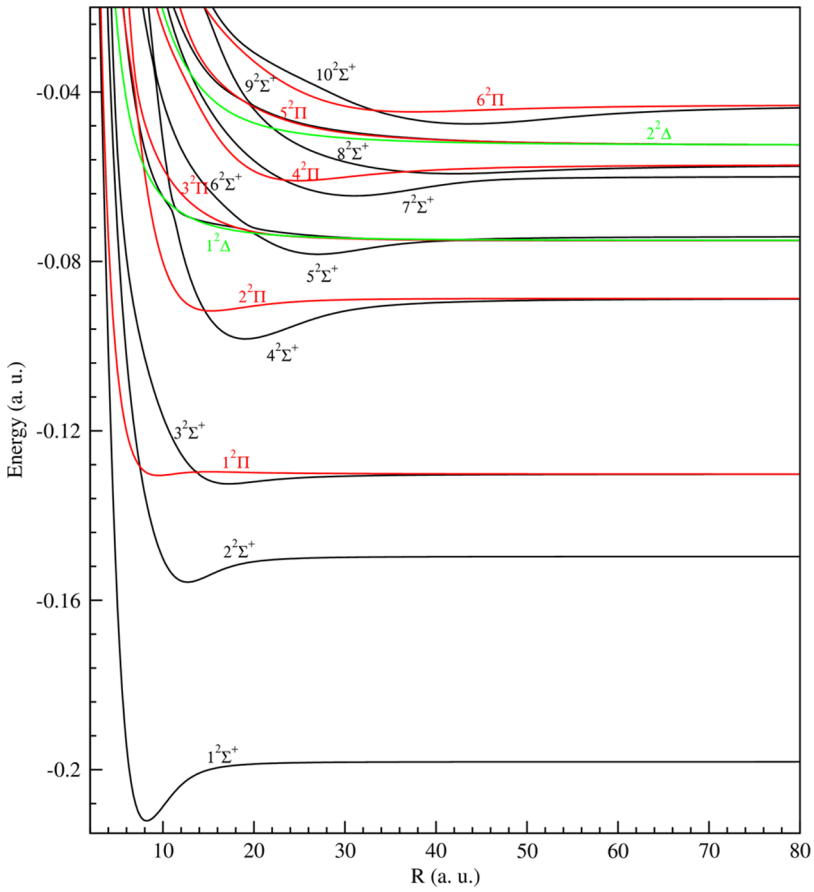

Figure 1. Potential energy curves of the first 18 electronic states of the charged diatomic system $FrLi^+$ dissociating into Fr(7s, 7p, 6d, 8s, and 8p) + Li^+ and Fr^+ + Li(2s, 2p, 3s, 3p, and 3d) include the $^2\Sigma^+$ (black line), $^2\Pi$ (red line), and $^2\Delta$ (blue line) states.

involving charged systems, including LiK^{+9}, NaK^{+12}, $LiRb^{+11}$, BeX^{2+} (X═H, Li, Na, K, Rb, and Cs),[26−28] BeH^{+30}, $BeLi^{+31}$ and SrH^{+32}. In the case of $FrLi^+$, we found avoided crossings between the electronic states $4^2\Sigma^+/5^2\Sigma^+$, $5^2\Sigma^+/6^2\Sigma^+$ and $8^2\Sigma^+/9^2\Sigma^+$ at distances of 11.20 au, 9.15, 19.50, and 42.27 au, and 19.17 au, respectively. For $FrNa^+$, avoided crossings were found between $4^2\Sigma^+/5^2\Sigma^+$ at 12.47 au, between $5^2\Sigma^+/6^2\Sigma^+$ at 33.65 au, and between $4^2\Pi/5^2\Pi$ at 12.32 au. Some of these avoided crossings are associated with the interaction between the energy curves, whereas others stem from the charge transfer processes between the $Fr^{(+)}X$ and $FrX^{(+)}$ (X = Li, Na) ionic systems.

From the adiabatic potential energies, we calculated the spectroscopic parameters for the charged diatomic systems $FrLi^+$ and $FrNa^+$, including the equilibrium distance (R_e), well depth (D_e), harmonic frequency (ω_e), anharmonicity constant ($\omega_e\chi_e$), and rotational constant (B_e). Tables 3 and 4 present these spectroscopic parameters for the ground and excited states of $^2\Sigma^+$, $^2\Pi$, and $^2\Delta$ symmetries. Currently, there are no available theoretical or experimental data for comparison. Hence, our work represents the first theoretical results for $FrLi^+$ and $FrNa^+$. To discuss our results, we compare the ground states of $FrLi^+$ and $FrNa^+$ with similar systems involving lithium, sodium, and other alkali atoms. For both charged systems, the ground state demonstrates the most profound potential well in contrast with the excited states or alternative symmetries. The equilibrium positions of $FrLi^+$ and $FrNa^+$ are 8.21 and 8.57 au, respectively, with corresponding potential wells measuring 3060 and 2941 cm^{-1}. Comparing these results with previous studies on heteronuclear alkali-charged systems,[8−11,16] $NaLi^+$ has the deepest well (8060 cm^{-1}) and the smallest equilibrium distance (6.37 au). The well depths of the ground states for LiK^{+9}, $LiRb^{+11}$, and $LiCs^{+16}$ are 4463, 3912, and 3176 cm^{-1}, respectively, with equilibrium positions at 7.34, 7.70, and 8.12 au. we observe a systematic decrease in well depths with increasing alkali atom mass, while equilibrium distances increase. Similar trends are found for NaK^{+12}, $NaRb^{+13}$, $NaCs^{+16}$, and $FrNa^+$ in terms of well depths and equilibrium distances in their ground states, which are 4442, 3718, 2979, and 2941 cm^{-1}, respectively, located at 7.75, 8.10, 8.51, and 8.57 au.

3.2. Transition Dipole Moments. To complete the electronic properties of charged diatomic systems $FrLi^+$ and $FrNa^+$, we calculated the dipole moments between states characterized by $^2\Sigma^+$ and $^2\Pi$ symmetries. These dipole moments are crucial for understanding the electric and optical properties of these molecules, including spontaneous and stimulated emissions, radiative charge exchange, and photo-association. Transition dipole moments have been previously calculated for other charged diatomic systems, such as LiK^{+9}, $LiRb^{+11}$, NaK^{+12}, $NaRb^{+13}$, K_2^{+14}, KRb^{+15}, $CsLi^+$, and $CsNa^{+16}$. Figures 3 and 4 illustrate the dipole moments across various electronic states: $1^2\sum^+$ to $2^2\sum^+$, $1^2\sum^+$ to $3^2\sum^+$, $1^2\sum^+$ to $4^2\sum^+$, $1^2\sum^+$ to $1^2\Pi$, $1^2\sum^+$ to $2^2\Pi$, $2^2\sum^+$ to $3^2\sum^+$, $2^2\sum^+$ to $4^2\sum^+$, and $2^2\sum^+$ to $2^2\Pi$ for each system. These figures exhibit comparable patterns to those identified in earlier previous studies.[9,11−13,15,16] Analysis of the data reveals that the significant transitions for both systems occur from $1^2\sum^+$ to $2^2\sum^+$ and

https://doi.org/10.1021/acsomega.3c06338
ACS Omega 2023, 8, 44977−44987

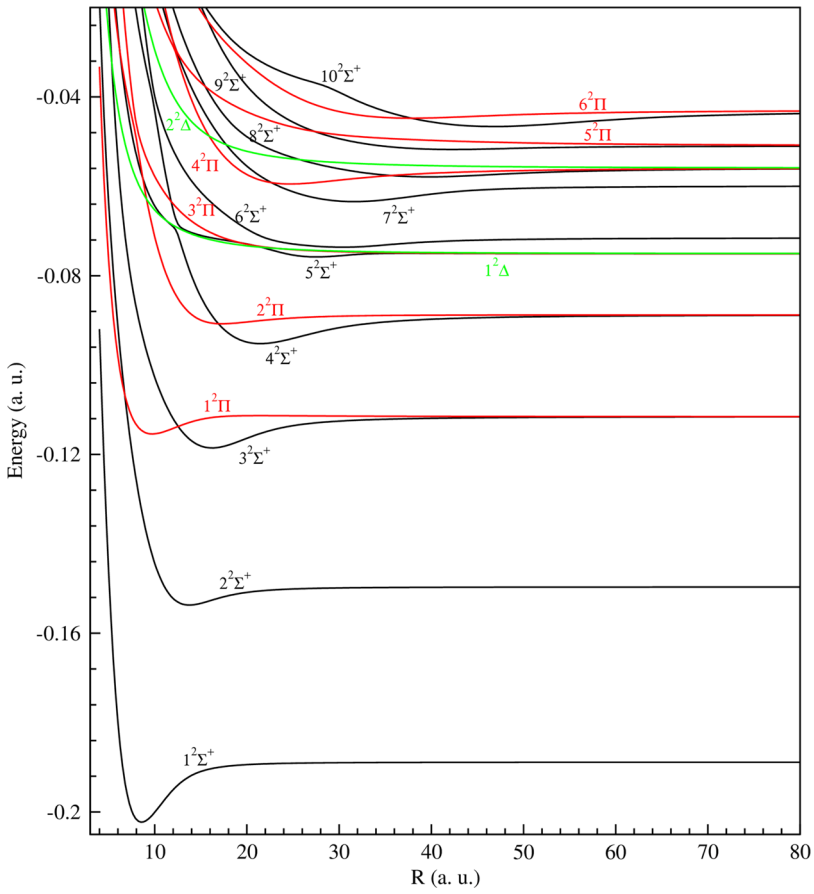

Figure 2. Potential energy curves of the first 18 electronic states of the charged diatomic system $FrNa^+$ dissociating into Fr(7s, 7p, 6d, 8s, and 8p) + Na^+ and Fr^+ + Na(3s, 3p, 4s, 3d, and 4p) include the $^2\Sigma^+$ (black line), $^2\Pi$ (red line), and $^2\Delta$ (blue line) states.

Table 3. Spectroscopic Parameters of the Attractive $^2\sum^+$ and $^2\Pi$ Electronic States of the Charged Diatomic System $FrLi^+$

state	R_e(au)	D_e(cm^{-1})	ω_e(cm^{-1})	$\omega_e\chi_e$(cm^{-1})	B_e(cm^{-1})
$1^2\sum^+$	8.21	3060	118.99	1.01	0.132677
$2^2\sum^+$	12.71	1328	62.03	0.65	0.055359
$3^2\sum^+$	17.25	502	30.11	2.29	0.030054
$4^2\sum^+$	19.07	2086	39.40	0.03	0.024591
$5^2\sum^+$	27.03	715	25.82	0.47	0.012204
$6^2\sum^+$	40.90	172	3.05	106.51	0.005346
$7^2\sum^+$	31.02	998	20.31	0.27	0.009293
$8^2\sum^+$	42.04	448	8.31	8.80	0.005106
$9^2\sum^+$	repulsive				
$10^2\sum^+$	43.58	976	13.64	0.05	0.004708
$1^2\Pi$	9.51	69	43.14	1.93	0.098883
$2^2\Pi$	15.31	634	31.84	0.62	0.038153
$3^2\Pi$	repulsive				
$4^2\Pi$	24.91	817	22.11	0.50	0.014412
$5^2\Pi$	repulsive				
$6^2\Pi$	37.49	360	8.23	19.44	0.006287

Table 4. Spectroscopic Parameters of the Attractive $^2\sum^+$ and $^2\Pi$ Electronic States of the Charged Diatomic System $FrNa^+$

state	R_e(au)	D_e(cm^{-1})	ω_e(cm^{-1})	$\omega_e\chi_e$(cm^{-1})	B_e(cm^{-1})
$1^2\sum^+$	8.57	2941	64.25	0.23	0.039301
$2^2\sum^+$	13.75	886	28.71	0.36	0.015277
$3^2\sum^+$	16.22	1535	26.11	0.13	0.010984
$4^2\sum^+$	21.45	1407	18.98	0.05	0.006279
$5^2\sum^+$	27.55	165	10.92	0.07	0.003807
$6^2\sum^+$	30.46	450	8.25	0.34	0.003115
$7^2\sum^+$	31.64	788	10.34	0.01	0.002886
$8^2\sum^+$	39.74	434	6.62	0.21	0.001829
$9^2\sum^+$	42.37	187	6.13	0.28	0.001609
$10^2\sum^+$	46.80	812	6.63	0.08	0.001319
$1^2\Pi$	9.73	848	32.67	0.16	0.030516
$2^2\Pi$	17.30	432	15.60	0.68	0.009650
$3^2\Pi$	repulsive				
$4^2\Pi$	24.71	783	12.42	0.38	0.004732
$5^2\Pi$	repulsive				
$6^2\Pi$	37.71	403	4.93	13.09	0.002010

from $2^2\sum^+$ to $4^2\sum^+$, with large magnitudes at short distances. These transitions reach maximum values of 3.18 and 4.51 atomic units at distances of 11.05 and 10.57 au for $FrLi^+$ and 3.41 and 4.13 atomic units at distances of 11.21 and 10.53 au for $FrNa^+$. The transitions from $1^2\sum^+$ to $3^2\sum^+$ and from $1^2\sum^+$ to $1^2\Pi$ increase rapidly at short distances and then become constant, equal to 2.33 atomic units for $FrLi^+$ and 2.42 atomic units for $FrNa^+$, respectively. These values align with the Li(2s) → Li(2p) and Na(3s) → Na(3p) atomic transitions, as confirmed by experimental data.[39] The same behavior was observed for the transitions from $2^2\sum^+$ to $4^2\sum^+$ and from $2^2\sum^+$ to $1^2\Pi$, which become constant equal to 2.74 atomic units for both systems. This value is consistent with the atomic transition Fr(7s) → Fr(7p). The other transition dipole

https://doi.org/10.1021/acsomega.3c06338
ACS Omega 2023, 8, 44977−44987

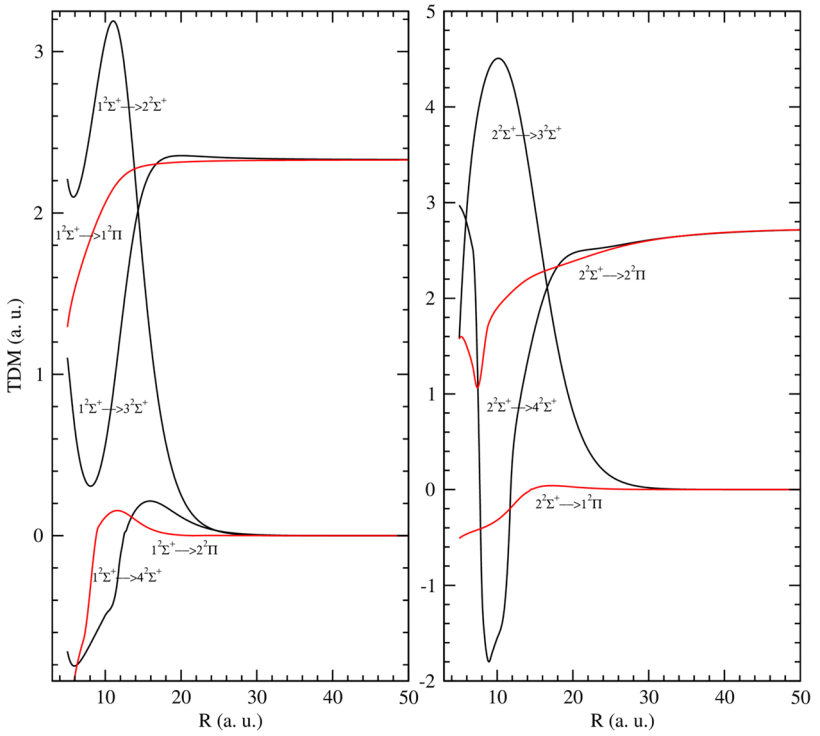

Figure 3. Transition dipole moments from the ground and first excited states to higher excited states of $^2\Sigma^+$ and $^2\Pi$ symmetries in the charged diatomic system $FrLi^+$.

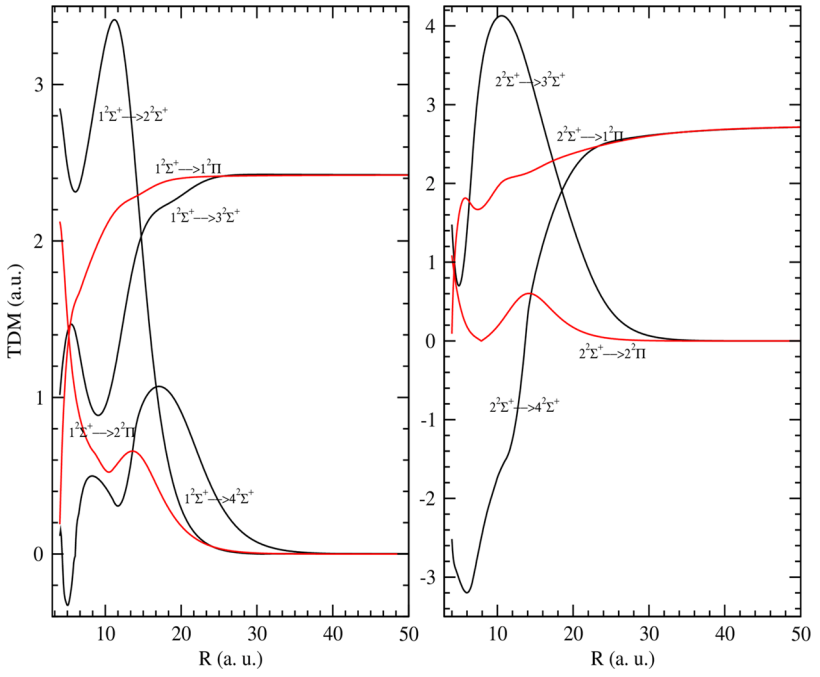

Figure 4. Transition dipole moments from the ground and first excited states to higher excited states of $^2\Sigma^+$ and $^2\Pi$ symmetries in charged diatomic system $FrNa^+$.

moments from $1^2\sum^+$ to $4^2\sum^+$, $1^2\sum^+$ to $2^2\Pi$, and $2^2\sum^+$ to $2^2\Pi$ are less significant and approach zero at larger distances due to the wave function behavior and dipole operator restrictions.

3.3. Vibrational States and Radiative Lifetimes. We employed a Fortran program that utilizes the Numerov algorithm[40] to calculate the vibrational levels for $1-3^2\sum^+$ states in each charged system. As inputs, we provide the minimum and maximum interatomic distances, the atomic mass of the atoms, the specified number of points, and the potential energies of the states under consideration. Figure 5 illustrates the calculated vibrational level spacing $(E_{v+1} - E_v)$ as a function of vibrational quantum number (v) for the $1-3^2\sum^+$ and $1^2\Pi$ states of $FrLi^+$ and $FrNa^+$ charged systems. For $FrLi^+$, the $1-3^2\sum^+$ and $1^2\Pi$ states encompassed 60, 53, 50, and 2 vibrational levels, respectively, while $FrNa^+$ exhibited 107, 82, 152, and 34 vibrational levels for the corresponding states.

https://doi.org/10.1021/acsomega.3c06338
ACS Omega 2023, 8, 44977−44987

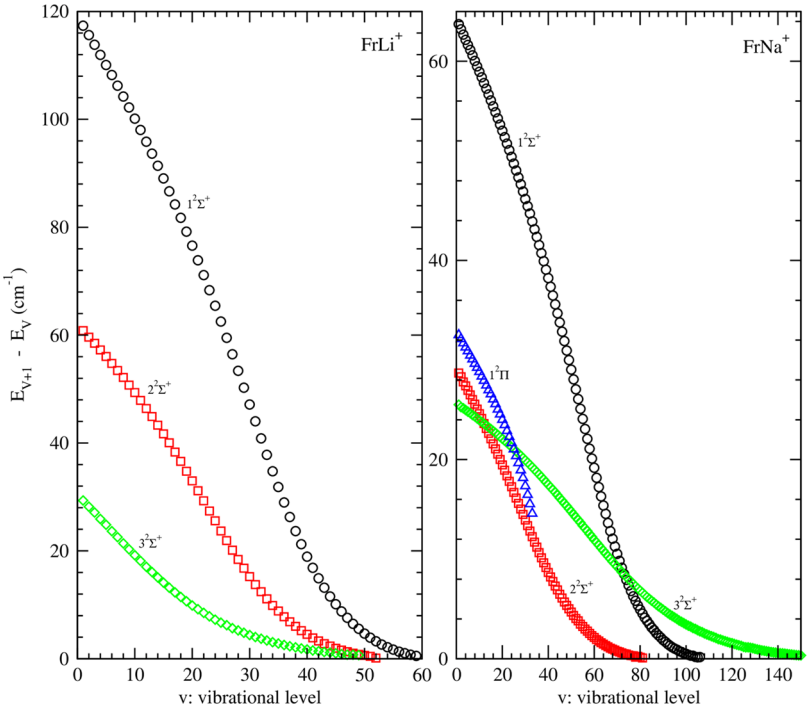

Figure 5. Vibrational level spacing $(E_{v+1} - E_v)$ as a function of vibrational quantum number (v) for the $1-3^2\sum^+$ and $1^2\Pi$ states of $FrLi^+$ and $FrNa^+$ charged systems.

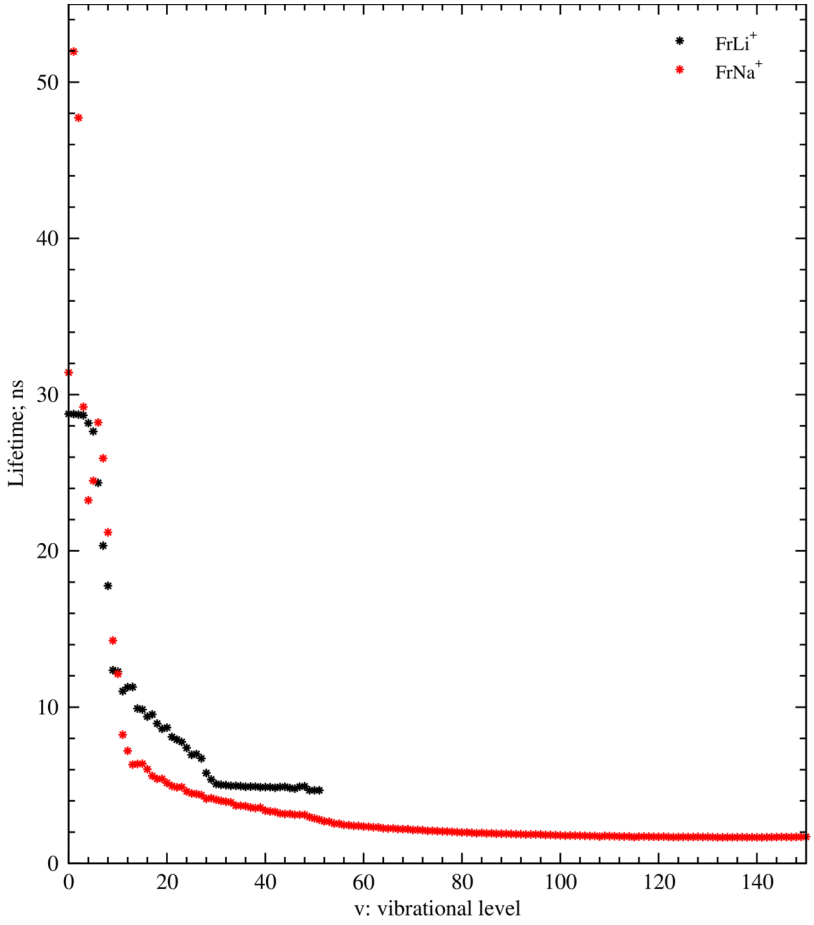

Figure 6. Radiative lifetimes of the vibrational states confined within the $2^2\Sigma^+$ state of $FrLi^+$ and $FrNa^+$ charged systems.

https://doi.org/10.1021/acsomega.3c06338
ACS Omega 2023, 8, 44977−44987

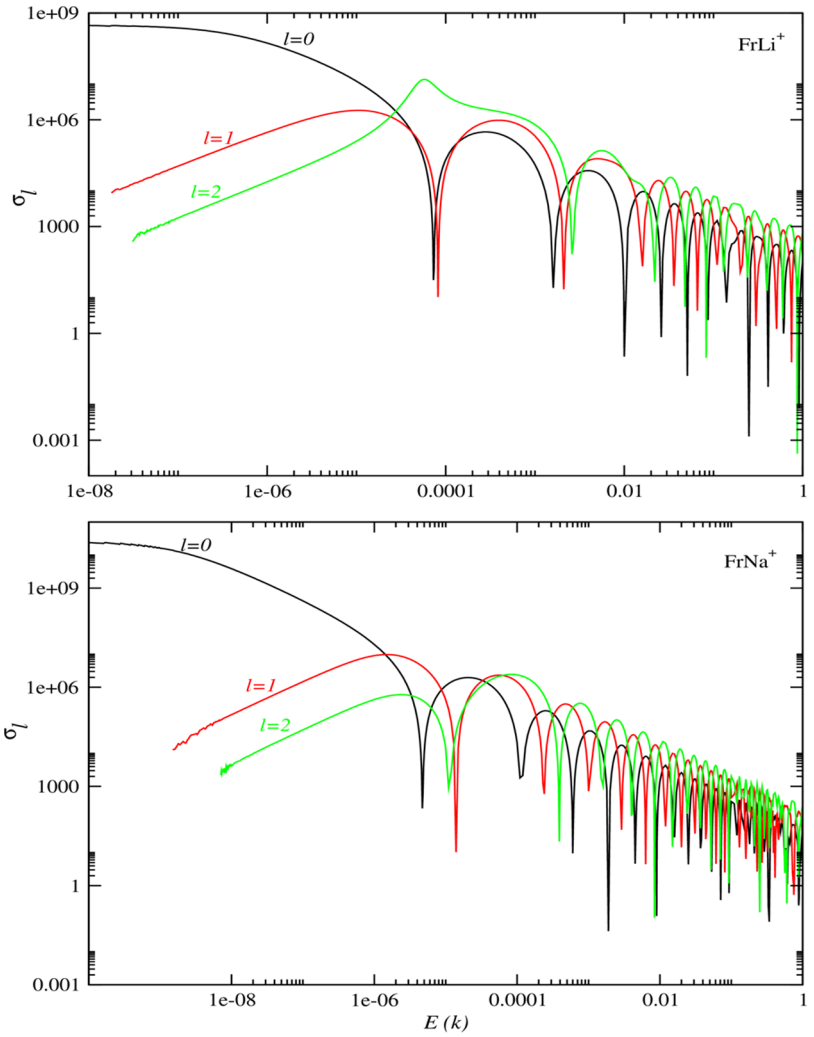

Figure 7. Partial-wave cross sections (in atomic units) as a function of collision energy E (in Kelvin) shown for $l = 0$ (black line), $l = 1$ (red line), and $l = 2$ (blue line). The top panel corresponds to the $Fr^+ + Li(2s)$ collision, while the bottom panel represents the $Fr^+ + Na(3s)$ collision. Both systems are in their ground state $X^2\Sigma^+$ potential.

The Golden Rule approximation serves as the basis for the calculation method employed to determine the radiative lifetimes. In the case of a specific vibration within an excited electronic state (e.g., $2^2\Sigma^+$), two distinct types of transitions are possible: bound-free and bound−bound transitions. The contribution bound-free transitions to the lifetime was precisely calculated by Franck−Condon approximation. Further details about the calculation procedure can be found in ref 41. To calculate the radiative lifetimes for a vibrational state of the $2^2\Sigma^+$ state, we utilized the potential energies of the $1^2\Sigma^+$ and $2^2\Sigma^+$ states, as well as the dipole functions connecting these two states. Figure 6 displays the radiative lifetimes of the vibrational states confined within the $2^2\Sigma^+$ state of the $FrLi^+$ and $FrNa^+$ charged systems. Remarkably, these radiative lifetimes fall within the nanosecond range, on average. In fact, the variation of the radiative lifetimes starts at 28.769 and 31.414 ns, respectively, for $FrLi^+$ and $FrNa^+$ in the first vibrational level ($v = 0$). Then, they increase and reach constant values of 4.677 and 1.690 ns, respectively, for $FrLi^+$ ($v = 51$) and $FrNa^+$ ($v = 152$). Previously, we conducted evaluations of radiative lifetimes for vibrational states confined within the $2^2\Sigma^+$ of LiY^+ (Y═K, Rb, and Cs)[42] and NaH^+[43] ionic molecules.

3.4. Elastic Scattering Properties. This section represents an extension of our theoretical investigation on collisions between ions and atoms.[44−47] We discuss the results obtained for low-energy elastic collisions between alkali atoms Li and Na and alkali ion Fr^+. It is assumed that the ion-atom collisions occur in the ground states of $FrLi^+$ and $FrNa^+$. In these states, the charged diatomic systems dissociate into $Fr^+ + Li(2s)$ and $Fr^+ + Na(3s)$, respectively. The discussion on the potential energy curves and spectroscopic characteristics of these states has already been covered earlier. The interaction potentials between an alkali ion and an alkali atom are typically usually constructed for three main distance regimes: short, intermediate, and long range.

The interaction potentials in the intermediate region are taken from our *ab initio* results, whereas an asymptotic expression is employed to express the interaction potential of ion-atom at large distances ($r > 20a_0$), where both species occupy their ground states. These two potential energy components are smoothly combined by using a spline function to determine the overall potential energy across the complete span of distances. The specific asymptotic expression used for the ion-atom interaction at large distances is as follows:

https://doi.org/10.1021/acsomega.3c06338
ACS Omega 2023, 8, 44977−44987

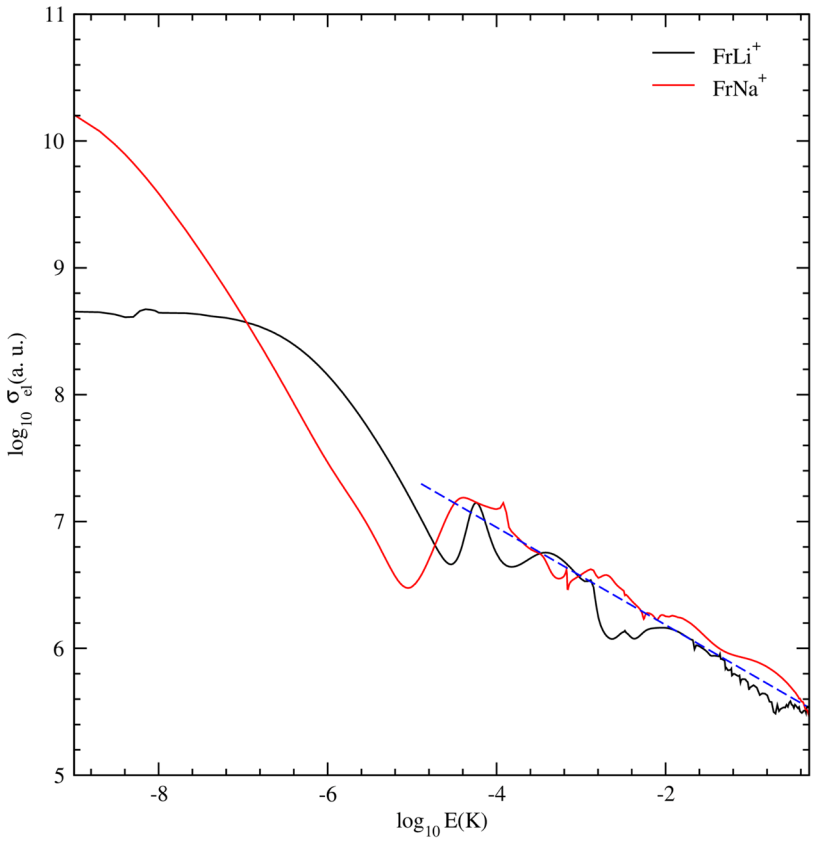

Figure 8. Logarithm of the total scattering cross section (in atomic units) plotted as a function of the logarithm of the energy E (in Kelvin) for ground state $X^2\Sigma^+$ of charged diatomic systems $(FrLi)^+$ and $(FrNa)^+$.

$$V(r) = -\frac{1}{2}\left(\frac{C_4}{r^4} + \frac{C_6}{r^6} + \ldots.\right) \tag{5}$$

where the dispersion coefficients C_4 and C_6 correspond to the dipole and quadrupole polarizabilities of the neutral atom being considered, which may refer to either Li(2s) or Na(3s). In this work, the dipole polarizabilities of Li(2s) and Na(3s) are taken to be equal to 160.61 and 162 au, respectively. r symbolizes the distance between the ion's center and the atom's center.

After calculating the asymptotic potential energy, the Numerov−Cooley algorithm[48] can be employed to determine the low and ultralow collisions properties. The radial Schrodinger equation that follows is solved to obtain the scattering wave function of the lth partial wave

$$\left[\frac{d^2}{dr^2} + k^2 - \frac{2\mu}{\hbar^2}V(r) - \frac{l(l+1)}{r^2}\right]\psi_l(kr) = 0 \tag{6}$$

where k represents the wavenumber associated with collisional energy $E = \frac{\hbar^2 k^2}{2\mu}$ and stands for the reduced mass of the ion-atom. The wave function $\psi_l(kr)$ presents the asymptotic form $\psi_l(kr) \sim \sin\left[kr - l\frac{\pi}{2} + \eta_l\right]$ with η_l representing the phase shift for lth partial wave. The total elastic scattering cross section is expressed as

$$\sigma_{el} = \frac{4\pi}{k^2}\sum_{l=0}^{\infty}(2l+1)\sin^2(\eta_l) \tag{7}$$

Primarily, we calculate the partial wave elastic scattering cross section of the ground state potential for the two charged diatomic systems $FrLi^+$ and $FrNa^+$. Figure 7 displays the partial-wave cross sections (in atomic units) for the $1^2\Sigma^+$ state of $FrLi^+$ and $FrNa^+$ at different collision energies (in Kelvin), corresponding to $l = 0$ (black line), $l = 1$ (red line), and $l = 2$ (blue line). The upper panel corresponds to the $Fr^+ + Li(2s)$ collision, while the lower panel represents the $Fr^+ + Na(3s)$ collision, with both systems in their ground state $X^2\Sigma^+$ potential. Comparing our results with partial wave elastic scattering cross sections of other charged diatomic systems,[44−47,49] we observe an identical behavior at low energy. This conformation can be attributed to the Wigner threshold law, which emerges from the analytic characteristics of the scattering wave functions during low-energy collisions. For both diatomic systems, the partial-wave cross section becomes energy-independent as k approaches 0 for $l = 0$, whereas it exhibits a linear variation for $l = 1$ and $l = 2$. Following the Wigner threshold laws, as k approaches zero, the phase shift for the lth partial wave behaves as $\eta_l \sim k^{2n+1}$ if $l < (n-3)/2$, while it follows $\eta_l \sim k^{n-2}$ for a long-range potential characterized by $1/r^4$. When the collision energies descend under 1 micro kelvin, a precise examination reveals that the charged diatomic systems progressively exhibit the characteristic Wigner threshold behavior. Within this regime, the s-wave cross section maintains its independence from energy, while higher-order partial waves exhibit a k^2 independence. In collisions between atoms and ions, the s-wave threshold behavior occurs at energies within the micro kelvin (μK) temperature range. However, for neutral alkali systems, this phenomenon manifests at energies near 100 μK, primarily attributed to a

https://doi.org/10.1021/acsomega.3c06338
ACS Omega 2023, 8, 44977−44987

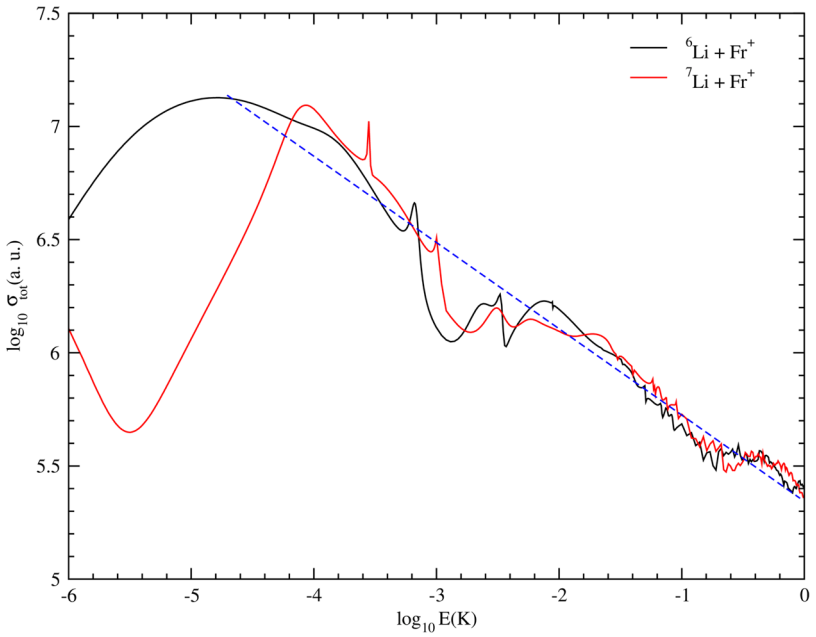

Figure 9. Logarithm of the total elastic scattering cross sections (σ_{tot}) (in atomic units) plotted against the logarithm of the energy E (in Kelvin) for both lithium isotopes ^{6}Li and ^{7}Li colliding with the francium ion $^{223}Fr^+$.

reduced range of van der Waals interactions among neutral atoms. Within the Wigner threshold regime, elastic collisions between heteronuclear atoms and ions prevail, with the charge transfer mechanism subdued. At low energies, the s-wave cross section displays a minimum, and outside the realm of the Wigner threshold law regime, the occurrence of the Ramsauer−Townsend effect,[50,51] could be attributed to this phenomenon.

Figure 8 shows the logarithm of the total elastic scattering cross sections (σ_{tot}) in atomic units plotted against the logarithm of the energy in Kelvin. The collisions involve the lithium atom (Li) or sodium atom (Na) with the francium ion (Fr^+), both in their ground states ($X^2\Sigma^+$). In the case of the charged diatomic systems $(FrLi)^+$ and $(FrNa)^+$, the total scattering cross section converges at high energies (E > 1 mK) and requires the contribution of several partial waves. With increasing collision energy, a greater number of partial waves contribute to the total cross section (σ_{tot}). It is important to highlight that the prevalence of the s-wave contribution becomes apparent at low energies, specifically when the temperature is less than 10^{-6} K. This phenomenon may be elucidated by the fluctuation in the altitude of the centrifugal barrier, which varies across different systems. Due to the variation in the interaction potential represented by C_4/r^4, the altitude of the centrifugal barrier is governed by $l(l+1)^{5/2}/(4C_4^{3/2}\mu^{5/2})$. Consequently, at energies under 1 μK, the influence of the inner region of the potential with higher partial waves is subdued by the centrifugal barrier. At high energies, the cross sections can be adequately characterized by power-law functions, as outlined below

$$\sigma_{tot} \sim \pi\left(\frac{\mu C_4^2}{\hbar^2}\right)\left(1+\frac{\pi^2}{16}\right)E^{-1/3} \quad (8)$$

By applying the logarithm function to eq 8, we obtain a linear relationship described by $\log \sigma_{tot}(E) = -\frac{1}{3}E + c_E$, where the intercept c_E depends on the coefficient C_4 of the potential, which is associated with the dipole polarizability. By conducting a numerical analysis and performing a linear regression using this equation in Figure 8, we proved that the slope of the line is approximately −0.333 for the $FrLi^+$ and $FrNa^+$ systems.

Ultimately, we examine the collision between the $^{223}Fr^+$ ion and the two lithium isotopes ^{6}Li and ^{7}Li at low energy. Figure 9 illustrates the logarithm of the total elastic scattering cross sections (σ_{tot}) (in atomic units) plotted against the logarithm of the energy (E) in Kelvin (K) for both lithium isotopes colliding with the francium ion $^{223}Fr^+$. The results indicate that the patterns are identical for ^{6}Li and ^{7}Li colliding with $^{223}Fr^+$, but they exhibit differences in magnitude, especially at low energies.

4. CONCLUSIONS

In this study, our objective was to investigate the electronic properties and elastic collisions of previously unexplored charged diatomic systems, specifically $FrLi^+$ and $FrNa^+$. We Employed a standard quantum chemistry approach using the pseudopotential method, Gaussian basis sets, and effective core polarization potentials. By successfully computing potential energies and spectroscopic parameters for various electronic states characterized by $^2\Sigma^+$, $^2\Pi$, and $^2\Delta$ symmetries, we systematically analyzed both charged diatomic systems. We identified and interpreted several avoided crossings within the higher $^2\Sigma^+$ and $^2\Pi$ states. Additionally, we calculated the transition dipole functions between electronic states characterized by $^2\Sigma^+$ and $^2\Pi$ symmetries. Furthermore, by leveraging the precise potential energies of the $X^2\Sigma^+$ and $2^2\Sigma^+$ states, along with the transition dipole functions between these states, we determined the radiative lifetimes of the vibrational states confined within the $2^2\Sigma^+$ state. Moreover, we utilized the accurate potential energy data to access the partial and total cross sections across a wide range of energies. Our findings indicated that at low energies (<1 mK), the elastic scattering cross section conformed to the Wigner law threshold behavior, while at high energies, the cross section scales as $E^{-1/3}$.

https://doi.org/10.1021/acsomega.3c06338
ACS Omega 2023, 8, 44977−44987

AUTHOR INFORMATION

Corresponding Authors

Chedli Ghanmi − *Laboratory of Interfaces and Advanced Materials, Faculty of Science, University of Monastir, 5019 Monastir, Tunisia;* orcid.org/0000-0002-5463-0708; Email: ghanmigfsm@gmail.com

Hamid Berriche − *Laboratory of Interfaces and Advanced Materials, Faculty of Science, University of Monastir, 5019 Monastir, Tunisia; Department of Mathematics and Physics, School of Arts and Sciences, Ras Al Khaimah American University, Ras Al Khaimah 10021, UAE;* Email: hamid.berriche@aurak.ac.ae

Complete contact information is available at: https://pubs.acs.org/10.1021/acsomega.3c06338

Notes

The authors declare no competing financial interest.

ACKNOWLEDGMENTS

This publication was supported by the Ministry of Higher Education and Scientific Research of Tunisia. The authors express their gratitude to the Ministry of Higher Education and Scientific Research of Tunisia for their support.

REFERENCES

(1) von Szentplay, L.; Fuentealba, P.; Preuss, H.; Stoll, H. Pseudopotential calculations on Rb_2^+, Cs_2^+, RbH^+, CsH^+ and the mixed alkali dimer ions. *Chem. Phys. Lett.* **1982**, *93*, 555−559, DOI: 10.1016/0009-2614(82)83728-7.

(2) Müller, W.; Meyer, W. Ground-state properties of alkali dimers and their cations (including the elements Li, Na, and K) from ab initio calculations with effective core polarization potentials. *J. Chem. Phys.* **1984**, *80*, 3311−3320.

(3) Valance, A.; Bernier, A.; Elmaddarsi, M. $\sum$ and Π molecular states for NaK^+, KRb^+ and $NaRb^+$ molecular ions. *Chem. Phys.* **1986**, *103*, 151−162.

(4) Magnier, S.; Millié, Ph. Potential curves for the ground and numerous highly excited electronic states of K_2 and NaK. *J. Phys. Rev. A* **1996**, *54*, 204−218.

(5) Romero, T.; Andrés, J. de.; Albertí, M.; Lucas, J. M.; Rubio, J.; Daudey, J. P.; Aguilar, A. Adiabatic and diabatic representations of potential energy curves for the $(NaRb)^+$ system. *Chem. Phys. Lett.* **1996**, *261*, 583−590, DOI: 10.1016/0009-2614(96)00993-1.

(6) Patil, S. H.; Tang, K. T. Simple model potential and model wave functions for $(H−alkali)^+$ and $(alkali−alkali)^+$ ions. *J. Chem. Phys.* **2000**, *113*, 676−681.

(7) Bouzouita, H.; Ghanmi, C.; Berriche, H. Ab initio study of the alkali-dimer cation Li_2^+. *J. Mol. Struct.: THEOCHEM* **2006**, *777*, 75−80.

(8) Berriche, H. Theoretical study of the lowest electronic states of the $LiNa^+$ molecule. *J. Mol. Struct.: THEOCHEM* **2003**, *663*, 101−108.

(9) Berriche, H.; Ghanmi, C.; Ben Ouada, H. Theoretical study of the electronic states and transition dipole moments of the LiK^+ molecule. *J. Mol. Spectrosc.* **2005**, *230*, 161−167, DOI: 10.1016/j.jms.2004.11.009.

(10) Ghanmi, C.; Berriche, H.; Ben Ouada, H. A vibrational level spacing analysis of the LiK^+ lowest electronic states: Long-range behavior and evaluation of Li and K polarizabilities. *Comput. Mater. Sci.* **2007**, *38*, 494−501.

(11) Ghanmi, C.; Farjallah, M.; Berriche, H. Theoretical study of low-lying electronic states of the $LiRb^+$ molecular ion: Structure, spectroscopy and transition dipole moments. *Int. J. Quantum Chem.* **2012**, *112*, 2403.

(12) Ghanmi, C.; Berriche, H.; Ben Ouada, H. Theoretical investigation of the molecular structure and transition dipole moments of the NaK^+ low lying electronic states. *J. Mol. Spectrosc.* **2006**, *235*, 158−165.

(13) Ghanmi, C.; Berriche, H.; Ben Ouada, H.Theoretical Investigation of the KRb^+ Ionic Molecule: Potential Energy, K and Rb Polarisabilities and Long-Range Behavior. In *Lecture Notes in Computer Science*; Springer, 2005; Vol. 4, pp 703−708.

(14) Ghanmi, C.; Bouzouita, H.; Mabrouk, N.; Berriche, H. Ab initio study of $NaRb^+$: Potential energy curves, spectroscopic constants and atomic polarizabilities. *J. Mol. Struct.: THEOCHEM* **2007**, *808*, 1−7.

(15) Berriche, H.; Ghanmi, C.; Farjallah, M.; Bouzouita, H. Theoretical investigation of the alkali-dimer cation K_2^+: Potential energy, dipole moment and atomic polarizabilities. *J. Comput. Methods Sci. Eng.* **2009**, *8*, 297−318.

(16) Ghanmi, C.; Bouzouita, H.; Berriche, H.; Ben Ouada, H. Theoretical investigation on $CsLi^+$ and $CsNa^+$ ionic molecules. *J. Mol. Struct.: THEOCHEM* **2006**, *777*, 81−86, DOI: 10.1016/j.theochem.2006.08.004.

(17) Lim, I. S.; Schwerdtfeger, P.; Sohnel, T.; Stoll, H. Ground-state properties and static dipole polarizabilities of the alkali dimers from K_2^n to Fr_2^n(n = 0,+1) from scalar relativistic pseudopotential coupled cluster and density functional studies. *J. Chem. Phys.* **2005**, *122*, No. 134307, DOI: 10.1063/1.1869979.

(18) Deiglmayr, J.; Aymar, M.; Wester, R.; Weidemüller, M.; Dulieu, O. Calculations of static dipole polarizabilities of alkali dimers: Prospects for alignment of ultracold molecules. *J. Chem. Phys.* **2008**, *129*, No. 064309, DOI: 10.1063/1.2960624.

(19) Aymar, M.; Dulieu, O.; Spiegelman, F. Electronic properties of francium diatomic compounds and prospects for cold molecule formation. *J. Phys. B: At., Mol. Opt. Phys.* **2006**, *39*, S905−S927.

(20) Jendoubi, I.; Ghanmi, C.; Berriche, H. Adiabatic and quasi-diabatic study of FrRb: structure, spectroscopy and dipole moments. *Theor. Chem. Acc.* **2016**, *135*, No. 142, DOI: 10.1007/s00214-016-1897-6.

(21) Jendoubi, I. Theoretical study of the FrLi molecule: computation of adiabatic and diabatic potential energy curves, spectroscopic constants, dipole moment, radiative lifetime and spectrum absorption. *Arab. J. Sci. Eng.* **2022**, *47*, 971−988.

(22) Jellali, S.; Habli, H.; Mejrissi, L.; Oujia, B.; Gadéa, F. X. Adiabatic and diabatic investigation of numerous electronic states for the alkali dimer FrNa. *J. Phys. Chem. A* **2019**, *123*, 544−555.

(23) Alyoussef, H.; Souissi, H.; Ben Hadj Ayed, M.; Alsahhaf, M. One and two electrons pseudo-potential investigation of the $(FrCs)^+$ and FrCs systems. *Arab J. Basic Appl. Sci.* **2020**, *27*, 456−470, DOI: 10.1080/25765299.2020.1848382.

(24) Souissi, H.; Mejrissi, L.; Habli, H.; Alsahhaf, M.; Oujia, B.; Gadéa, F. X. Ab initio diabatic and adiabatic calculation for the francium hydride FrH. *New J. Chem.* **2020**, *44*, 5572−5587, DOI: 10.1039/C9NJ06391A.

(25) Shandalau, M.; Lamberti, P. Relativistic ab initio study on the spectroscopic and radiative properties of the lowest states and modeling of the optical cycles for the LiFr molecule. *J. Quant. Spectrosc. Radiat. Transfer* **2023**, *296*, No. 108467, DOI: 10.1016/j.jqsrt.2022.108467.

(26) Ghanmi, C.; Farjallah, M.; Alshamrani, R.; Berriche, H. Theoretical investigation of the $BeRb^{2+}$, $BeCs^{2+}$ and $SrRb^{2+}$ Dications. *Russ. J. Phys. Chem. A* **2021**, *95*, S109−S119.

(27) Ghanmi, C.; Farjallah, M.; Berriche, H.; Al-sehemi, A. G. Structure and electronic properties of the doubly charged diatomic dications BeX^{2+} (X = Na and K). *Can. J. Phys.* **2016**, *94*, 1−8.

(28) Farjallah, M.; Ghanmi, C.; Berriche, H. Theoretical investigation of the low-lying electronic states of the ionic molecules BeH^{2+}: Potential energy curves, spectroscopic constants, vibrational levels and transition dipole moments. *Russ. J. Phys. Chem. A* **2012**, *86*, 1226.

(29) Farjallah, M.; Ghanmi, C.; Berriche, H. Theoretical investigation of the low-lying electronic of the ae hydride ion $BeLi^{2+}$: Potential energy curves, spectroscopic constants, vibrational levels and transition dipole moments. *J. Comput. Methods Sci. Eng.* **2010**, *10*, 139−147.

(30) Farjallah, M.; Ghanmi, C.; Berriche, H. Structure and spectroscopic properties of the Beryllium hydride BeH^+: Potential energy curves, spectroscopic constants, vibrational levels and permanent dipole moments. *Eur. Phys. J. D* **2013**, *67*, No. 245, DOI: 10.1140/epjd/e2013-40141-3.
(31) Ghanmi, C.; Farjallah, M.; Berriche, H. Theoretical study of the alkaline-earth $(LiBe)^+$ion: structure, spectroscopy and dipole moments. *J. Phys. B: At., Mol. Opt. Phys.* **2017**, *50*, No. 055101.
(32) Belayouni, S.; Ghanmi, C.; Berriche, H. Adiabatic and quasi-diabatic investigation of the strontium hydride cation SrH^+: structure, spectroscopy and dipole moments. *Can. J. Phys.* **2016**, *94*, 791−802.
(33) Mabrouk, N.; Zrafi, W.; Berriche, H. Theoretical study of the LiNa molecule beyond the Born−Oppenheimer approximation: adiabatic and diabatic potential energy curves, radial coupling, adiabatic correction, dipole moments and vibrational levels. *Mol. Phys.* **2020**, *118*, No. e1605098.
(34) Zrafi, W.; Ladjimi, H.; Said, H.; Berriche, H.; Tomza, M. Ab initio electronic structure and prospects for the formation of ultracold calcium-alkali-metal-atom molecular ions. *New J. Phys.* **2020**, *22*, No. 073015.
(35) Durand, Ph.; Barthelat, J. C. A theoretical method to determine atomic pseudopotentials for electronic structure calculations of molecules and solids. *Theor. Chim. Acta* **1975**, *38*, 283−302.
(36) Müller, W.; Flesh, J.; Meyer, W. Treatment of intershell correlation effects in ab initio calculations by use of core polarization potentials. Method and application to alkali and alkaline earth atoms. *J. Chem. Phys.* **1984**, *80*, 3297−3310, DOI: 10.1063/1.447083.
(37) Foucrault, M.; Millie, Ph.; Daudey, J. P. Nonperturbative method for core−valence correlation in pseudopotential calculations: Application to the Rb_2 and Cs_2 molecules. *J. Chem. Phys.* **1992**, *96*, 1257−1264.
(38) Moore, C. E. *Atomic Energy Levels*, NSRDS-NBS No. 467; US Governoment Printing Office: WA, 1989.
(39) Partridge, H.; Langhoff, R. S. Theoretical treatment of the X $^1\sum^+$, A $^1\sum^+$, and B $^1\Pi$ states of LiH. *J. Chem. Phys.* **1981**, *74*, 2361−2371.
(40) Fox, L. *The Numerical Solution of Two-Boundary Value Problems in Ordinary Differential Equations*; Oxford University Press: London, 1957.
(41) Mabrouk, N.; Berriche, H. Theoretical study of the NaLi molecule: Potential energy curves, spectroscopic constants, dipole moments and radiative lifetimes. *J. Phys. B: At., Mol. Opt. Phys.* **2008**, *41*, No. 155101.
(42) Ghanmi, C.; Berriche, H. Radiative lifetimes of LiK^+, $LiRb^+$ and $LiCs^+$ in the $2^2\sum^+$ state. *AIP Conf. Proc.* **2009**, *1148*, 321−326, DOI: 10.1063/1.3225305.
(43) Berriche, H. One-electron pseudopotential study of the alkali hydride cation NaH^+: Structure, spectroscopy, transition dipole moments, and radiative lifetimes. *Int. J. Quantum Chem.* **2013**, *113*, 1003.
(44) Ladjimi, H.; Sardar, D.; Farjallah, M.; Alharzali, N.; Naskar, S.; Mlika, R.; Berriche, H.; Deb, B. Spectroscopic properties of the molecular ions BeX^+ (X = Na, K, Rb): Forming cold molecular ions from an ion-atom mixture by stimulated Raman adiabatic process. *Mol. Phys.* **2018**, *116*, 1812−1826.
(45) Bellaouini, S.; Pal, A.; Rakshit, A.; Farjallah, M.; Deb, B.; Berriche, H. Structure, spectroscopy and cold collisions of the $(SrNa)^+$ ionic system. *Eur. Phys. J. D* **2018**, *72*, No. 131, DOI: 10.1140/epjd/e2018-90054-6.
(46) Rakshit, A.; Ghanmi, C.; Berriche, H.; Deb, B. Interactions and low-energy collisions between an alkali ion and an alkali atom of a different nucleus. *J. Phys. B: At., Mol. Opt. Phys.* **2016**, *49*, No. 105202.
(47) Ladjimi, H.; Zrafi, W.; Farjallah, M.; Bejaoui, M.; Berriche, H. Electronic structure, cold ion-atom elastic collision properties and possibility of laser cooling of $BeCs^+$ molecular ion. *Phys. Chem. Chem. Phys.* **2022**, *24*, 18511−18522.
(48) Cooley, J. W. An improved eigenvalue corrector formula for solving the Schrödinger equation for central fields. *Math. Comput.* **1961**, *15*, 363−374, DOI: 10.2307/2003025.
(49) Bouchelaghem, F.; Bouledroua, M. Charge transfer cross sections and transport coefficients of $^{39}K^+-^{39}K$ and $^{41}K^+-^{39}K$ at low-energy. *AIP Adv.* **2023**, *13*, No. 025159, DOI: 10.1063/5.0134588.
(50) Mitroy, J.; Bromley, M. W. J. Semiempirical calculation of van der Waals coefficients for alkali-metal and alkaline-earth-metal atoms. *Phys. Rev. A* **2016**, *68*, No. 052714, DOI: 10.1103/PhysRevA.68.052714.
(51) Reid, D. D.; Wadehra, J. M. Scattering of low-energy electrons and positrons by atomic beryllium: Ramsauer−Townsend effect. *J. Phys. B: At., Mol. Opt. Phys.* **2014**, *47*, No. 225211.

https://doi.org/10.1021/acsomega.3c06338
ACS Omega 2023, 8, 44977−44987